


# Flexible one-structure arched triboelectric nanogenerator based on common electrode for high efficiency energy harvesting and self-powered motion sensing

Cite as: AIP Advances **8**, 045022 (2018); <https://doi.org/10.1063/1.5027659>

Submitted: 05 March 2018 . Accepted: 15 April 2018 . Published Online: 26 April 2018

Xi Chen , Jian He, Linlin Song, Zengxing Zhang, Zhumei Tian , Tao Wen, Cong Zhai, Yi Chen, Jundong Cho, Xiujian Chou, and Chenyang Xue 



View Online



Export Citation



CrossMark

## ARTICLES YOU MAY BE INTERESTED IN

[Motion behavior of water droplets driven by triboelectric nanogenerator](#)

Applied Physics Letters **112**, 183701 (2018); <https://doi.org/10.1063/1.5030152>

[Waterproof and stretchable triboelectric nanogenerator for biomechanical energy harvesting and self-powered sensing](#)

Applied Physics Letters **112**, 203902 (2018); <https://doi.org/10.1063/1.5028478>

[A nanowire based triboelectric nanogenerator for harvesting water wave energy and its applications](#)

APL Materials **5**, 074104 (2017); <https://doi.org/10.1063/1.4977216>

Don't let your writing  
keep you from getting  
published!

AIP | Author Services

Learn more today!



## Flexible one-structure arched triboelectric nanogenerator based on common electrode for high efficiency energy harvesting and self-powered motion sensing

Xi Chen,<sup>1,a</sup> Jian He,<sup>1,a</sup> Linlin Song,<sup>2</sup> Zengxing Zhang,<sup>3</sup> Zhumei Tian,<sup>1,4</sup> Tao Wen,<sup>1</sup> Cong Zhai,<sup>1</sup> Yi Chen,<sup>1</sup> Jundong Cho,<sup>1,5</sup> Xiujian Chou,<sup>1,b</sup> and Chenyang Xue<sup>1,b</sup>

<sup>1</sup>Science and Technology on Electronic Test and Measurement Laboratory, North University of China, Taiyuan 030051, China

<sup>2</sup>State Key Laboratory for Space Power-Sources Technology, Shanghai 201620, China

<sup>3</sup>Department of Micro and Nano Systems Technology, University College of Southeast Norway, Horten 3184, Borre, Norway

<sup>4</sup>Department of Electronics, Xinzhou Teachers University, Xinzhou 034000, China

<sup>5</sup>Department of Electrical and Electronic Engineering, Sungkyunkwan University, Suwon 16419, South Korea

(Received 5 March 2018; accepted 15 April 2018; published online 26 April 2018)

Triboelectric nanogenerators are widely used because of low cost, simple manufacturing process and high output performance. In this work, a flexible one-structure arched triboelectric nanogenerator (FOAT), based on common electrode to combine the single-electrode mode and contact-separation, was designed using silicone rubber, epoxy resin and flexible electrode. The peak-to-peak short circuit current of 18 $\mu$ A and the peak-to-peak open circuit voltage of 570V can be obtained from the FOAT with the size of 5 $\times$ 7 cm<sup>2</sup> under the frequency of 3Hz and the pressure of 300N. The peak-to-peak short circuit current of FOAT is increased by 29% and 80%, and the peak-to-peak open circuit voltage is increased by 33% and 54% compared with single-electrode mode and contact-separation mode, respectively. FOAT realizes the combination of two generation modes, which improves the output performance of triboelectric nanogenerator (TENG). 62 light-emitting-diodes (LEDs) can be completely lit up and 2.2 $\mu$ F capacitor can be easily charged to 1.2V in 9s. When the FOAT is placed at different parts of the human body, the human motion energy can be harvested and be the sensing signal for motion monitoring sensor. Based on the above characteristics, FOAT exhibits great potential in illumination, power supplies for wearable electronic devices and self-powered motion monitoring sensor via harvesting the energy of human motion. © 2018 Author(s). All article content, except where otherwise noted, is licensed under a Creative Commons Attribution (CC BY) license (<http://creativecommons.org/licenses/by/4.0/>). <https://doi.org/10.1063/1.5027659>

### I. INTRODUCTION

With the popularity of electronic technology in daily life, wearable devices gradually tend to be miniaturized, intelligent and versatile, such as the Samsung Galaxy Gear, NIKE+, Google glasses and so on.<sup>1,2</sup> Batteries used as traditional power supply for wearable devices are limited, it is difficult to ensure uninterrupted power supply for wearable devices. In order to extend the battery life, one effective strategy is to use self-powered system for wearable devices.<sup>3,4</sup> At present, to harvest energy efficiently, researchers mainly study piezoelectric effect,<sup>5–7</sup> triboelectric effect,<sup>8–11</sup> thermoelectric effect,<sup>12,13</sup> photoelectric effect,<sup>14,15</sup> electromagnetic effect<sup>16,17</sup> and hybrid generator.<sup>18</sup>

<sup>a</sup>Xi Chen and Jian He contributed equally to this work.

<sup>b</sup>Authors to whom any correspondence should be addressed E-mail: [chouxiujian@nuc.edu.cn](mailto:chouxiujian@nuc.edu.cn) and [xuechenyang@nuc.edu.cn](mailto:xuechenyang@nuc.edu.cn)

Triboelectric effect is a common natural phenomenon and has been discovered long time ago, while it is often recognized as a negative effect in daily life. In recent years, triboelectric nanogenerators (TENGs) based on the coupling between contact electrification and electrostatic induction were proposed and designed by Wang Zhong Lin's group.<sup>19–22</sup> As a new energy harvesting method, considering its relatively high output voltage and easy fabrication process, TENGs **have** get attention by researchers, which have been widely applied in the harvesting of wind energy,<sup>23,24</sup> ocean water energy,<sup>25,26</sup> human motion energy<sup>27–29</sup> and vibration energy.<sup>30</sup> In particular, mechanical energy exists extensively in human motion and can be effectively harvested by TENGs, which attracts more and more researchers. Converting the energy of the human body motion into electrical energy has been used in the various fields of energy source for self-powered electronics,<sup>31,32</sup> healthcare devices,<sup>33</sup> active sensor monitoring of human movement<sup>34</sup> and so on. However, most materials of previously reported of TENGs' electrodes are metal or rigid, which don't have the ability of bending and stretching and are not suitable for direct contact with human skin.<sup>35</sup> In addition, most of the existing TENGs adopt single generating mode, limiting output performance.<sup>36,37</sup> Therefore, it is necessary to design a flexible, biocompatible and high-performance triboelectric nanogenerator.

In this paper, a flexible one-structure arched triboelectric nanogenerator (FOAT) is fabricated, which integrates two power generation modes: single-electrode mode and contact-separation mode based on common electrode. To realize good flexibility of FOAT, we selected silicone rubber and epoxy resin as the materials of friction layers and fabricated the flexible electrodes. Furthermore, the pyramid surface microstructures of silicone rubber can increase the contact area to improve the output performance of FOAT. The thickness and the weight of the whole structure is about 9mm and 42g respectively, which can collect tiny human motion. And during the pressing and releasing at the frequency of 3Hz and the pressure of 300N, the FOAT with a size of 5×7cm<sup>2</sup> produces a maximum peak-to-peak short circuit current of 18μA and a maximum peak-to-peak open circuit voltage of 570V. FOAT can simultaneously power 62 light-emitting-diodes (LEDs) and harvest various forms of human motion as angle sensor and jump height sensor when placed at arm joint or under the foot, which manifests the broad prospects in illuminating, self-powered wearable devices and motion monitoring sensor.

## II. EXPERIMENTAL SECTION

### A. Materials preparation

We used silicone rubber, epoxy resin (type AB), and flexible electrodes as the based materials. The ratio of silicone rubber and curing agent was 50:1 and the mixture was heating for 2 hours at 80°C. The ratio of epoxy resin A and epoxy resin B was 1:1 and the epoxy resin cured after 24 hours at room temperature. The materials of flexible electrodes were silver-plated copper powder and solid silicone rubber, and flexible electrodes were prepared by the method of vulcanization.

### B. Fabrication of flexible electrodes

Fig. 1(a) shows the fabrication process of flexible electrodes. The silver-plated copper powder was mixed into the solid silicone rubber, then the mixture was vulcanized and heated at the 160°C for 20 minutes later. Then the mixture was removed from plate vulcanizing press machine and cooled to room temperature. The flexible electrodes we prepared had good electrical conductivity and stretch ability.

### C. Fabrication of FOAT

FOAT mainly contains two generation modes: single-electrode mode and contact-separation mode by a common electrode. Single-electrode mode consists of silicone rubber as friction layer and a flexible electrode as upper electrode. Contact-separation mode consists of silicone rubber and epoxy resin as friction layers and a flexible electrode as lower electrode. The upper electrode is the common electrode of two generation modes.

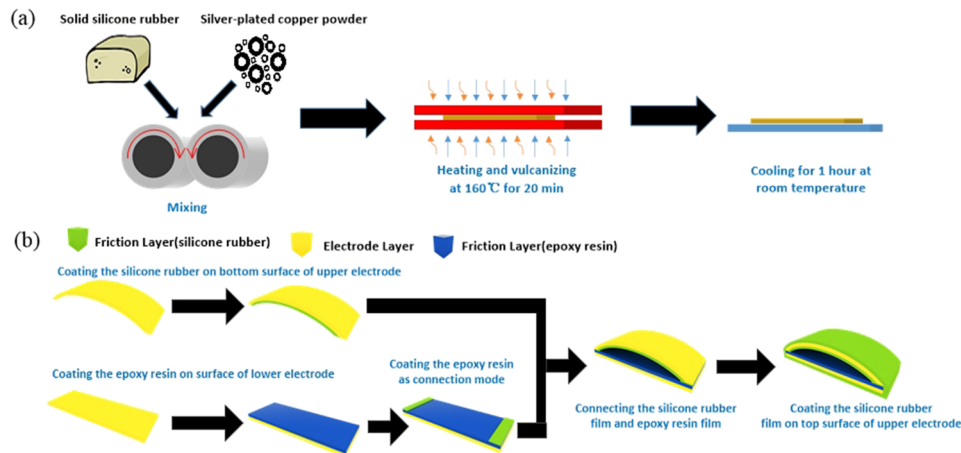


FIG. 1. (a) The fabrication process of flexible electrode using solid silicone rubber and silver-plated copper powder. (b) The manufacture process of FOAT by silicone rubber, epoxy resin and flexible electrodes.

The fabrication process of FOAT is shown in Fig. 1(b). First, silicone rubber film of  $700\mu\text{m}$  was coated on the bottom surface of upper electrode through the arch mold. Second, a thin epoxy resin film of  $700\mu\text{m}$  was coated on lower electrode. Third, a small amount of silicone rubber was applied on both sides of the epoxy resin as the connection mode for upper electrode and lower electrode, which could connect the silicone rubber layer and epoxy resin layer. Finally, on the top surface of the upper flexible electrode, a silicone rubber film was processed with a thickness of  $700\mu\text{m}$  by the arch mold. Before the silicone rubber cured, the sand paper with pyramid structure had been placed on the surface of the silicone rubber film. After the silicone rubber film cured, sand paper was peeled off from the silicone rubber film. The pyramid structure will be prepared on the surface of the silicone rubber film.

#### D. Device characterization

The photography of the surface of silicone rubber films and flexible electrodes were analyzed by SEM. The deformation ( $\Delta d$ ) of silicone rubber, epoxy resin and flexible electrode was tested by HANDPI HP-500 spiral tension machine. The resistance of flexible electrode was measured by Tektronix model DMM4050 6-1/2 Digit Precision Multimeter. To explore output performances of single-electrode mode, contact-separation mode and FOAT, we used digital source meter (Keithley 6514 electrometer). A linear motor was used to simulate the relative motion of the palm skin to a linear motor. Because the abilities to attract charges of sheepskin and palm skin are similar, we chose the sheepskin instead of palm skin in the process of experiment. The sheepskin was fixed at the free end of the linear motor and the FOAT was fixed at the fixed end of the linear motor to simulate the process of hand pressing FOAT. A diagram of the testing process is shown in Fig. S1 in [supplementary material](#). We used the pressure sensor (QLMH-P) and high speed response display instrument (QL-8016) to detect and display the pressure information of the linear motor.

### III. RESULTS AND DISCUSSION

#### A. Structure and working principle of FOAT

FOAT is a flexible one-structure arched triboelectric nanogenerator, as is schematically showed in Fig. 2(a). The digital photography of FOAT is depicted in Fig. 2(b). The SEM image of the surface structure of the rubber is shown in Fig. 2(c). The SEM images of the surface for electrode made by rubber and silver-plated copper powder is shown in Figs. 2(d) and 2(e), respectively. Since the materials of FOAT are soft, stretchable and fully flexible, it is possible to revert to the original shape after bending at different angles (shown in Fig. 2(f)). To demonstrate the tensile property of silicone

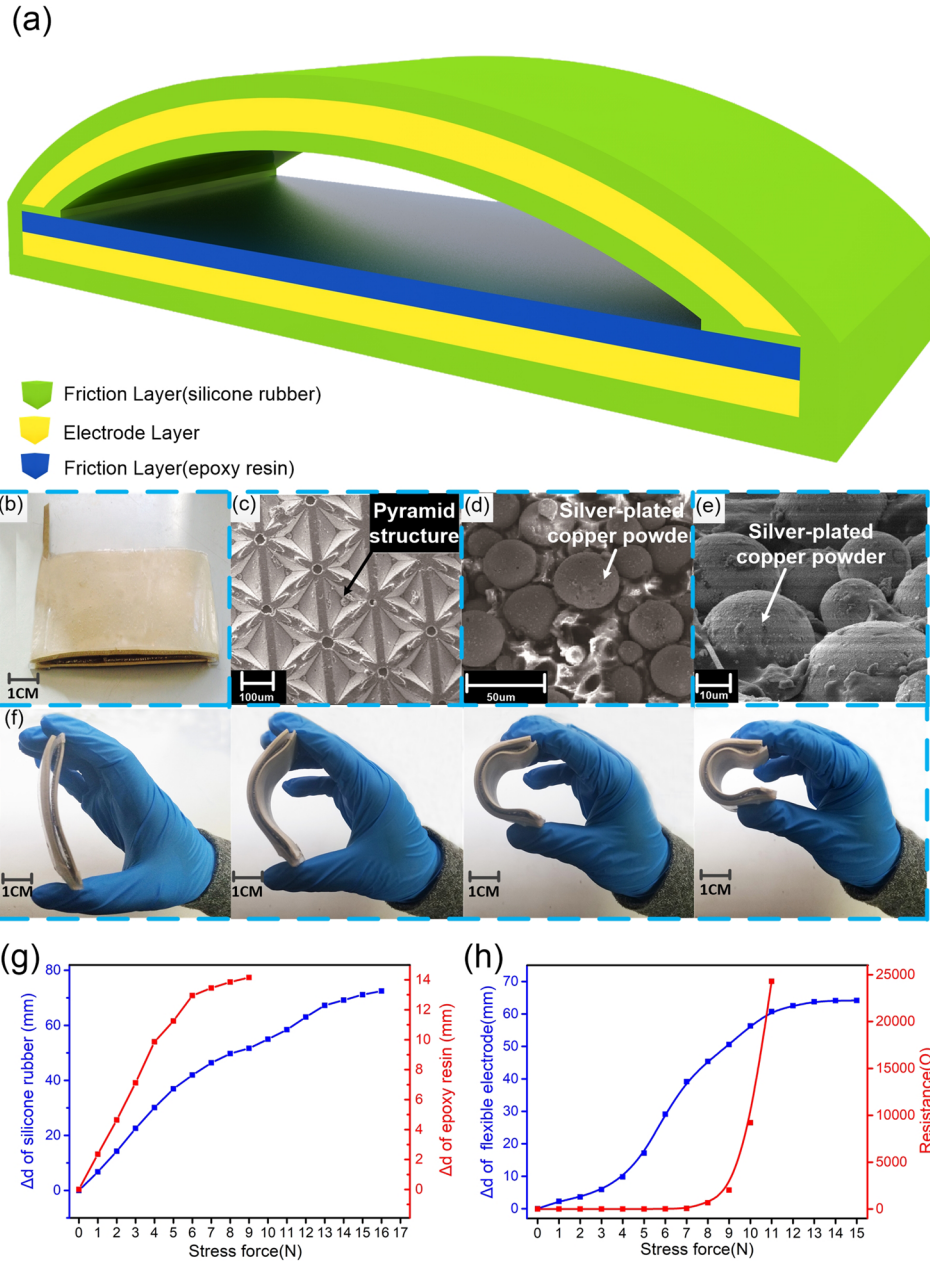


FIG. 2. The structure and characteristics of materials of FOAT. (a) The schematic illustration of the structure of FOAT. (b) Digital photography of FOAT. (c) SEM image of the silicone rubber. (d) and (e) SEM images of the flexible electrode surface. (f) Photos of FOAT being bent at different angles. (g) The deformation ( $\Delta d$ ) of the rubber and epoxy resin with the increase of stress force. (h) The deformation ( $\Delta d$ ) of the electrode and the resistance with the increase of stress force.

rubber, epoxy resin and flexible electrode, the relations between deformation ( $\Delta d$ ) and stress force are measured by spiral tension machine. For the silicone rubber, epoxy resin and flexible electrode samples with the thickness of  $700\mu\text{m}$  and the length of  $60\text{mm}$  can be stretched  $70\text{mm}$ ,  $13\text{mm}$  and  $60\text{mm}$  respectively until being snapped (Figs. 2(g) and 2(h)). Meanwhile, the resistance of flexible electrode is measured. When the deformation ( $\Delta d$ ) of flexible electrode is in the range of  $0$  to  $65\text{mm}$ , the resistance keeps mostly unchangeable, which illustrates that the electrode has good electrical conductivity and stretch ability. And the resistance rapidly increases when the deformation ( $\Delta d$ ) of flexible electrode is exceeded  $50\text{mm}$ , which signifies that the flexible electrode gradually loses

electrical conductivity (Fig. 2(h)). Because materials of FOAT are flexible and have good bending ability and resilience, FOAT is a fully flexible triboelectric nanogenerator.

FOAT combines the work principle of single-electrode mode and contact-separation mode, as shown in Fig. 3. The working principle of the single-electrode mode is shown in Fig. 3(a). Firstly, skin will contact with silicone rubber film which is the surface of the single-electrode mode. Because skin is much more triboelectrically positive than silicone rubber, electrons will be transferred from skin into silicone rubber, which generates positive charges on the surface of skin and negative charges on the surface of silicone rubber (Fig. 3(a-i)). As the skin separates from silicone rubber film,

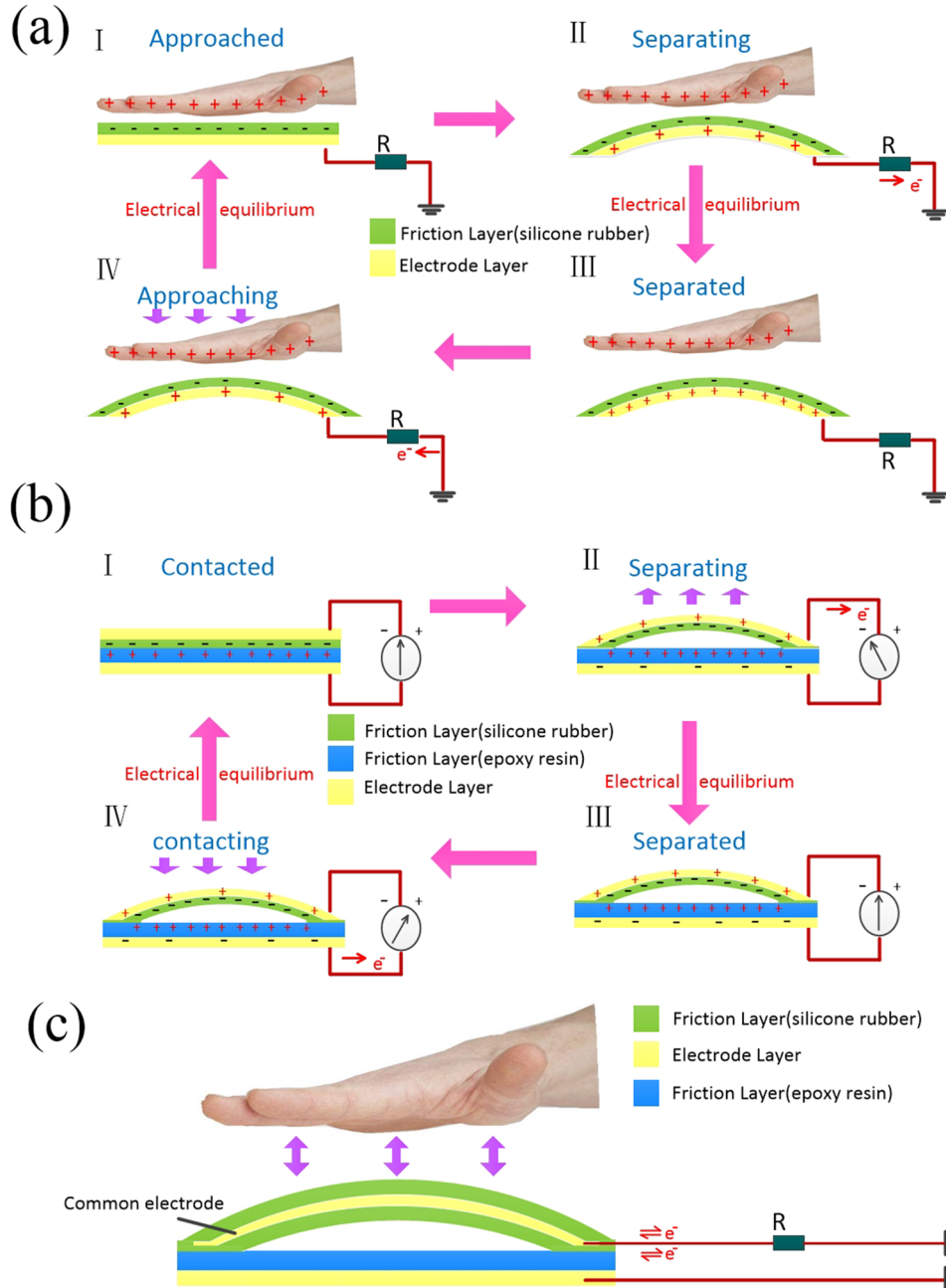


FIG. 3. Schematic diagrams of the working mechanism for generation process. (a) Working mechanism of single-electrode mode which is contacted with palm skin (b) Working mechanism of contact-separation mode (c) Working mechanism of FOAT.

an electric potential is produced, which drives electrons flow from flexible electrode to the ground until reaches an electrostatic equilibrium (Fig. 3(a-ii)). When the skin and the silicone rubber film getting closer, the opposite electric potential will appear (Fig. 3(a-iii)). Consequently, electrons will flow from ground to electrode and reach an electrostatic equilibrium again (Fig. 3(a-iv)). This is a cycle of single-electrode mode operation. The principle of the contact-separation mode is shown in Fig. 3(b). When the force from hand is applied on the single-electrode mode to make the friction layers of the contact-separation mode contact with each other, electrons will be injected from epoxy resin into the silicone rubber (Fig. 3(b-i)). With the pressure being released, the silicone rubber film and epoxy resin film will be separated, electric potential is established between the two electrodes and the electrons will flow from upper electrode to lower electrode. As the space between the two electrodes increases, the electric potential between electrodes eventually reaches an equilibrium (Fig. 3(b-ii)). When the FOAT is pressed again, the electric potential decreases as the friction layers get closer to each other. The electrons will transfer from lower electrode to upper electrode (Fig. 3(b-iii)), achieving a new equilibrium (Fig. 3(b-iv)). This is a cycle of contact-separation mode operation. Thus, when the hand presses and separates from FOAT, the periodicity current and voltage from single-electrode mode and contact-separation mode can be generated.

The key point of FOAT is a common electrode. By using the common electrode, it is possible to realize the integration of the single-electrode mode and the contact-separation mode, transferring the generation charges of the two modes at the same time (Fig. 3(c)). In the generation process of FOAT, since the surface of rubber can acquire more negative charges from the skin and epoxy resin friction layers, more electrons were transferred between the common electrode and the ground. In other words, compared to the traditional single-electrode mode or contact-separation mode, the output performance of FOAT can be greatly improved.

## B. Output characterization of FOAT

The peak-to-peak short circuit current and the peak-to-peak open circuit voltage can be measured by a linear motor to imitate the skin contact and separation with FOAT. When the size of FOAT is  $5 \times 7 \text{ cm}^2$ , the peak-to-peak short circuit current of single-electrode mode and contact-separation mode is about  $14 \mu\text{A}$  and  $10 \mu\text{A}$  (Figs. 4(a) and 4(b)) respectively, under the frequency of 3Hz and the pressure of 300N. The peak-to-peak open circuit voltages of single-electrode and contact-separation are about 430V and 370V (Figs. 4(d) and 4(e)), respectively. The peak-to-peak short circuit current and peak-to-peak open circuit voltage of FOAT are about  $18 \mu\text{A}$  and 570V (Figs. 4(c) and 4(f)). Compared with the independent generation mode, the peak-to-peak short circuit current is increased by 29% and 80% and the peak-to-peak open circuit voltage is increased by 33% and 54%, (Fig. 4(g)). The reason is that the common electrode plays a significant role in adding up the amount of transferred charges from the surfaces of friction layers, which enhances the output current and voltage. When the hand presses and separates from FOAT, contact electrification and electrostatic induction of two generation modes do not happen at the same moment. The contact between hand and silicone rubber film surface will be little earlier than that of the two surfaces of contact-separation mode. Charge transfer takes place in the circuit of single-electrode mode, and then charge transfer occurs in the circuit of contact-separation mode. Consequently, the peak output current and voltage will not appear at the same time and the outputs of FOAT are not the linear superposition of each mode. As shown in Fig. 4(h), reversibility of FOAT is analyzed by the repeated application of pressure using a linear motor. The short circuit current doesn't have obvious decrease before and after 3000 pressing cycles with the pressure of 300N. As a consequence, during the palm's constantly pressing, FOAT can produce a larger output current and voltage.

The size of contact surface is the key factor for the output current of FOAT. Under the same conditions of 3Hz and 300N, when the size of FOAT increases from  $2 \times 4$ ,  $3 \times 5$ ,  $4 \times 6$  to  $5 \times 7 \text{ cm}^2$ , the output current increases from 6, 8, 15 to  $18 \mu\text{A}$ , respectively as shown in Fig. 5(a). This phenomenon is can be explained that more electric charges from bigger contact surface generate higher electric potential. Therefore, more charges are required to balance this electric potential, which causes current increase.

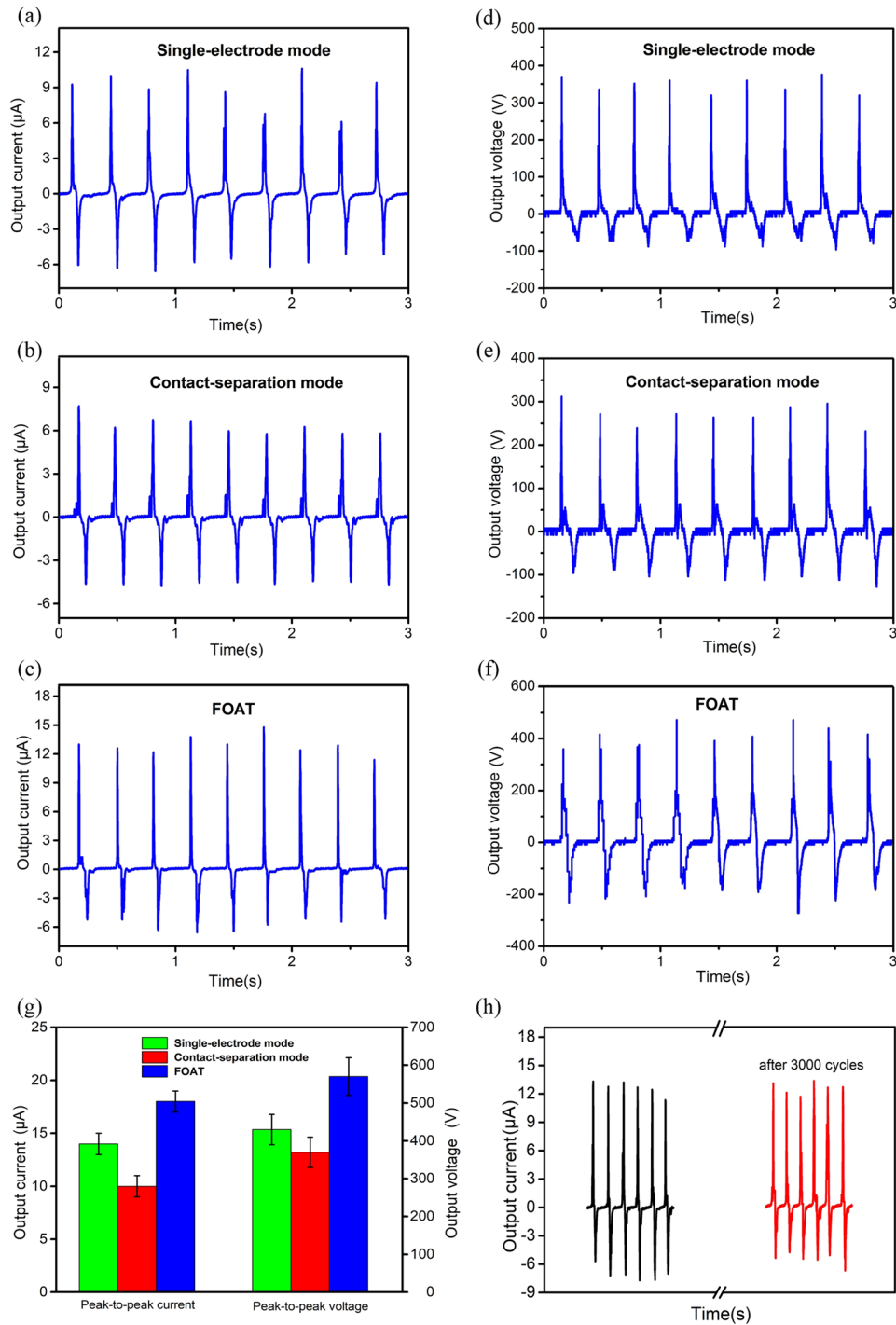


FIG. 4. Output performance of single-electrode mode, contact-separation mode and FOAT. (a)-(c) Short circuit current with time based on single-electrode mode, contact-separation mode and FOAT. (d)-(f) Open circuit current with time based on single-electrode mode, contact-separation mode and FOAT. (g) The comparison of output performance for single-electrode mode, contact-separation mode and FOAT. (h) The output performance before and after 3000 cycles.

Changing the pressure on the FOAT is also one way to improve the output performance of the generator. With the frequency of 3Hz and size of  $5 \times 7 \text{cm}^2$ , when the pressures are increased from 100, 200 to 300N, the corresponding output currents are increased from 6, 8 to  $15 \mu\text{A}$ , respectively as shown in Fig. 5(b). The reason is that more pressure leads to the closer contact between the two



friction surfaces. As a consequence, the more positive and negative charges will be accumulated on the contact surface, which causes an increase of current.

The press frequency also affects the output performance of FOAT. As is shown in Fig. 5(c), the output current of FOAT, experiences an obvious increased trend with the increase of the frequency for the pressure of 300N and same size. Under different frequencies ranging from 1 Hz to 3 Hz, the enhanced output currents of 3, 8, 14  $\mu\text{A}$  are obtained. This phenomenon can be explained that more charges are generated on the contact surface since the contacting and separating time become shorter with the higher frequency, which causes the higher output current.

To more systematically describe the impedance characteristics of FOAT as a generator, FOAT with the size of  $5 \times 7 \text{ cm}^2$  is connected with the resistance range from 1 to  $10^9 \Omega$ . As illustrated in Fig. 5(d), the output voltage shows an obvious increase with the increase of load resistance. In addition, the instantaneous power ( $P$ ) of FOAT calculated by  $P=U^2/R$  (where  $R$  is the load resistance

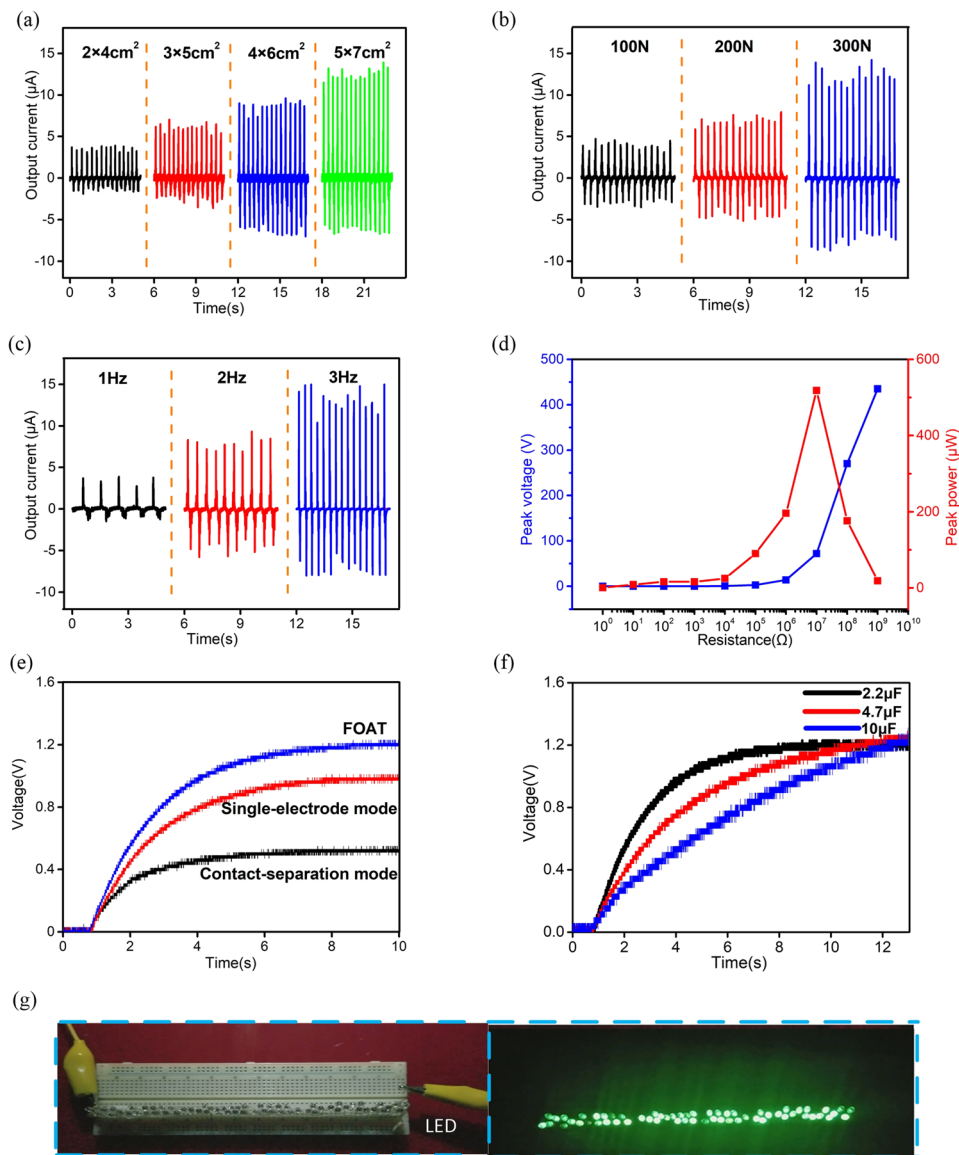


FIG. 5. (a) Short circuit current under different sizes of FOAT. (b) Short circuit current under different pressures of FOAT. (c) Short circuit current under different pressure frequencies of FOAT. (d) The peak power with different load resistance. (e) The charge curves of the single-electrode mode, contact-separation mode and FOAT for a capacitor. (f) The charging curves of FOAT for 2.2, 4.7 and  $10 \mu\text{F}$  capacitors. (g) 62 green LEDs lit up were during the slapping.

and  $U$  is the output voltage corresponding to different load resistances such 1, 10, 100 $\Omega$  and so on) has a significant increase from 1 to 10<sup>7</sup>  $\Omega$ . By contrast, the instantaneous power ( $P$ ) exhibits a decrease from 10<sup>7</sup> to 10<sup>9</sup>  $\Omega$ . And the peak of instantaneous power occurs at about 518 $\mu$ W, corresponding to the peak surface energy density of 14.8  $\mu$ W/cm<sup>2</sup>. It should be noted that the surface energy density is defined by  $W=P/S$ , where  $P$  is the peak power when the FOAT was connected with external resistance. When the external resistance is about 10<sup>7</sup> $\Omega$  and the size of FOAT is 5  $\times$  7 cm<sup>2</sup>, the energy density is 14.8  $\mu$ W/cm<sup>2</sup>.

### C. Power applications of FOAT

Fig. 5(e) demonstrates the charging performances of two individual modes and FOAT. 2.2 $\mu$ F capacitor can be easily charged to 0.9, 0.4 and 1.2V in 9s. The charging voltage of FOAT is higher than that of the single-electrode mode and contact-separation mode. FOAT has the fastest charging rate compared with any one of two modes when the 2.2 $\mu$ F capacitor is charged to the same voltage. Besides, in order to describe the charging rate for different capacitors, 2.2, 4.7 and 10 $\mu$ F capacitors we chose could be charged up to 1.2V in around 8, 10 and 13s, respectively (Fig. 5(f)). Therefore, it is evident that FOAT can greatly enhance device performance under the same conditions and has an enormous potential as a new type of TENG.

In order to more clearly illustrate the application of FOAT, we use FOAT to light up the array of green LEDs. 62 green LEDs connected serially can be illuminated during the slapping the FOAT by hand, and normal walking can also drive 62 LEDs when FOAT was placed under the foot (Fig. 5(g), the Videos S1 and S2 of the [supplementary material](#)). As a consequence, FOAT has a bright prospect in illumination and power supplies for wearable electronic devices.

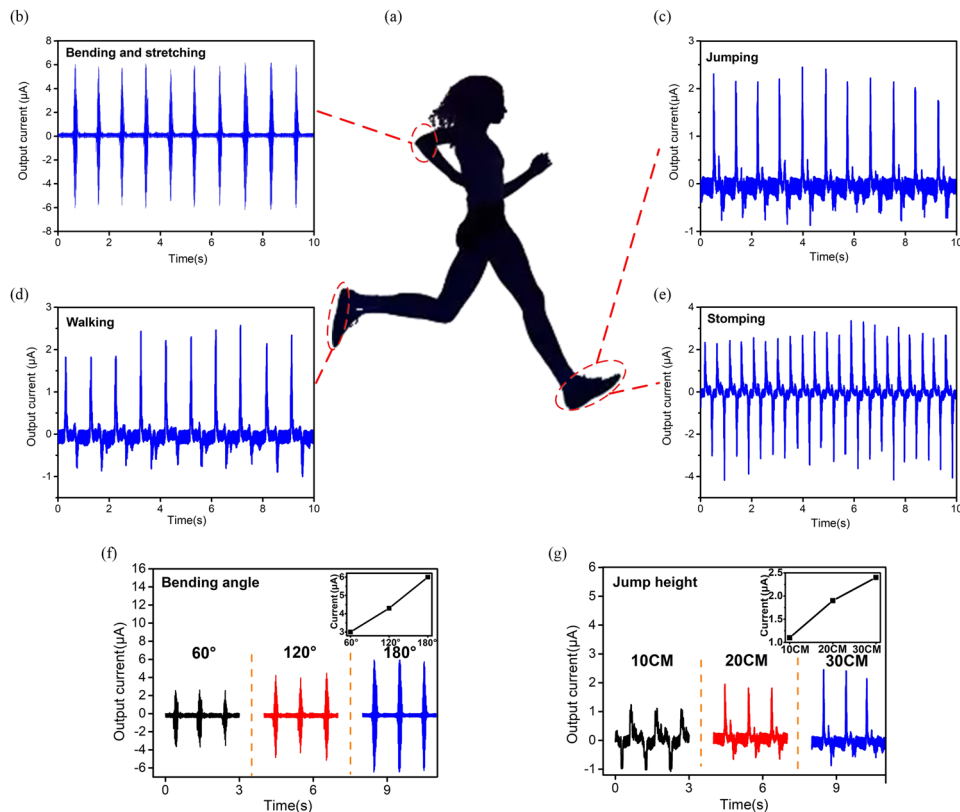


FIG. 6. The application of FOAT in harvesting motion energy as a motion monitoring sensor. (a) The schematic of FOAT placed at elbow joint and under the foot. (b) Output current of the arm bent and stretched periodically. (c)-(e) Output current of FOAT when a person jumping, walking and stomping. (f) Output current of the FOAT under different bending angles. (g) Output current of the FOAT under different jump heights.

#### D. Sensor applications of FOAT

FOAT is soft, flexible and stretchable, which is suitable to contact with skin directly. When FOAT is placed at elbow joint and under the foot, the mechanical energy of movement can be harvested, which can be used as a sensing signal for a motion monitoring sensor to monitor gesture (Fig. 6(a)). As the elbow joint is periodically bent, the obtained output current is shown in Fig. 6(b) and the Video S3 of the [supplementary material](#). With FOAT placed under the foot, when a person is jumping, walking and stomping, the output currents are different, as illustrated in Figs. 6(c)–6(e) and the Videos S4–S6 of the [supplementary material](#). In addition, by distinguishing the output current, they can also be used as a motion monitoring sensor. Fig. 6(f) presents the output current increasing from 2, 4.3 to  $6\mu\text{A}$  corresponding to bending angle of  $60^\circ$ ,  $120^\circ$  to  $180^\circ$ , which is used as an angle sensor. The frequency and the pressure on the FOAT are roughly constant during the movement of the arm, so the output current of the sensor will not be obviously affected by the frequency and pressure. Fig. 6(g) demonstrates the output current of 1, 1.8 and  $2.4\mu\text{A}$  for the different jump height from 10, 20 to 30cm, which can be a jump height sensor for body motion sensing. To measure the jump height more accurately, it is necessary to recalibrate for different frequencies and different people with different weights when FOAT is put into practical application. It is obvious that FOAT can generate different output current with different bending angle and jump height, and there is a good linear relationship between the output current and the bending angle as well as jump height. As a result, the function of FOAT is not only to harvest the motion energy of the human body as a power source, but also to be used as a motion monitoring sensor to gesture monitor and health monitor. Since the materials of FOAT are fully flexible and stretchable, it is indicated that FOAT has good biocompatibility, and is suitable for being a power source for wearable electronic devices and a new type of human motion monitoring sensor.

#### IV. CONCLUSIONS

In summary, we introduced a flexible one-structure arched triboelectric nanogenerator (FOAT), which is a new type of energy device that can be used to harvest the energy from human motion. To realize the integration of the single-electrode mode and the contact-separation mode, we designed the common electrode which transferred the charges from the two modes to enhance the energy generation performance of TENG. Besides, the working principle of FOAT and output performance were illustrated. The peak-to-peak short circuit current of  $18\mu\text{A}$  and the peak-to-peak open circuit voltage of 570V could be obtained from the FOAT with a size of  $5*7\text{ cm}^2$  at a frequency of 3Hz and a pressure of 300N. In addition, the influences of different sizes, pressures and pressure frequencies on output performance and their causes were analyzed and explained. 62 LEDs could be driven and  $2.2\mu\text{F}$  could be easily charged to 1.2V in 9s. FOAT can also be a motion monitoring sensor to monitor gesture, when it is placed at elbow joint and under the foot. Because the characteristics of FOAT are soft, fully flexible, stretchable and biocompatibility, FOAT has a broad application prospect, such as wearable electronics, illumination and motion monitoring sensor.

#### SUPPLEMENTARY MATERIAL

See [supplementary material](#) for Figure S1—Supporting figure of illustrating the testing process by using a linear motor to imitate human movement, Video S1—Supporting video of 62 LEDs lighted using FOAT when the palm continually presses the FOAT, Video S2—Supporting video of 62 LEDs lighted using FOAT when stomping (fixed under the foot), Video S3—Supporting video of output signal when the arm is bent and stretched periodically (fixed at the elbow joint), Video S4—Supporting video of output signal when a person is jumping (fixed under the foot), Video S5—Supporting video of output signal when a person is walking (fixed under the foot), and Video S6—Supporting video of output signal when a person is stomping (fixed under the foot).

#### ACKNOWLEDGMENTS

This work was supported by the National Science Foundation of China (Grant No. 61525107, 51422510, 51675493, 51605449), Shanxi Province Applied Fundamental Research Program

(201601D021064), the National High Technology Research and Development (863) Program of China (Grant No. 2015AA042601), National Natural Science Foundation of China as National Major Scientific Instruments Development Project (Grant No. 61727806) and Shanxi “1331 Project” Key Subject Construction (1331KSC), School Foundation for North University of China (Grant No. 110246).

- <sup>1</sup> T. Zhou, C. Zhang, C. B. Han, F. R. Fan, W. Tang, and Z. L. Wang, *ACS Appl. Mater. Interfaces* **6**, 14695 (2014).
- <sup>2</sup> G. Zhu, B. Peng, J. Chen, Q. Jing, and Z. L. Wang, *Nano Energy* **14**, 126 (2014).
- <sup>3</sup> F. R. Fan, L. Lin, G. Zhu, W. Wu, R. Zhang, and Z. L. Wang, *Nano Lett.* **12**, 3109 (2012).
- <sup>4</sup> P. Bai, G. Zhu, Y. Liu, J. Chen, Q. Jing, W. Yang, J. Ma, G. Zhang, and Z. L. Wang, *ACS Nano* **7**, 6361 (2013).
- <sup>5</sup> S. Crossley, R. A. Whiter, and S. Kar-Narayan, *Mater. Sci. Technol.* **30**, 1613 (2014).
- <sup>6</sup> M. Zhang, T. Gao, J. Wang, J. Liao, Y. Qiu, Q. Yang, H. Xue, Z. Shi, Y. Zhao, Z. Xiong, and L. Chen, *Nano Energy* **13**, 298 (2015).
- <sup>7</sup> J. Lim, H. Jung, C. Baek, G. T. Hwang, J. Ryu, D. Yoon, J. Yoo, K. Il Park, and J. H. Kim, *Nano Energy* **41**, 337 (2017).
- <sup>8</sup> K. Dong, J. Deng, Y. Zi, Y. C. Wang, C. Xu, H. Zou, W. Ding, Y. Dai, B. Gu, B. Sun, and Z. L. Wang, *Adv. Mater.* **29** (2017).
- <sup>9</sup> Q. T. Xue, Z. Wang, H. Tian, Y. Huan, Q. Y. Xie, Y. Yang, D. Xie, C. Li, Y. Shu, X. H. Wang, and T. L. Ren, *AIP Advances* **5**, 017102 (2015).
- <sup>10</sup> X. S. Zhang, M. Di Han, R. X. Wang, F. Y. Zhu, Z. H. Li, W. Wang, and H. X. Zhang, *Nano Lett.* **13**, 1168 (2013).
- <sup>11</sup> L. Zhang, L. Jin, B. Zhang, W. Deng, and H. Pan, *Nano Energy* **16**, 516 (2015).
- <sup>12</sup> Y. Yang, Z. H. Lin, T. Hou, F. Zhang, and Z. L. Wang, *Nano Res.* **5**, 888 (2012).
- <sup>13</sup> Y. Xie, T. M. Chou, W. Yang, M. He, Y. Zhao, N. Li, and Z. H. Lin, *Semicond. Sci. Technol.* **32**, 0 (2017).
- <sup>14</sup> G. Zhang, K. Zhang, Q. Yin, X. F. Jiang, Z. Wang, J. Xin, W. Ma, H. Yan, F. Huang, and Y. Cao, *J. Am. Chem. Soc.* **139**, 2387 (2017).
- <sup>15</sup> Q. Tang, H. Zhang, B. He, and P. Yang, *Nano Energy* **30**, 818 (2016).
- <sup>16</sup> A. Nammari, S. Doughty, D. Savage, L. Weiss, A. Jaganathan, and H. Bardaweel, *Microsyst. Technol.* **23**, 4645 (2017).
- <sup>17</sup> X. Wang and Y. Yang, *Nano Energy* **32**, 36 (2017).
- <sup>18</sup> Z. X. Zhang, J. He, J. Q. Han, H. Y. Xu, J. L. Mu, T. Wen, D. W. Wang, Z. M. Tian, Z. T. Chen, and C. Y. Xue, *Sci. China Technol. Sci.* **60**, 1068 (2017).
- <sup>19</sup> G. Zhu, C. Pan, W. Guo, C. Y. Chen, Y. Zhou, R. Yu, and Z. L. Wang, *Nano Lett.* **12**, 4960 (2012).
- <sup>20</sup> S. Wang, L. Lin, and Z. Lin, *Nano Energy* **11**, 436 (2015).
- <sup>21</sup> F. R. Fan, Z. Q. Tian, and Z. L. Wang, *Nano Energy* **1**, 328 (2012).
- <sup>22</sup> Z. L. Wang, *ACS Nano* **7**, 9533 (2013).
- <sup>23</sup> Z. Wen, J. Chen, M. H. Yeh, H. Guo, Z. Li, X. Fan, T. Zhang, L. Zhu, and Z. L. Wang, *Nano Energy* **16**, 38 (2015).
- <sup>24</sup> S. Chen, C. Gao, W. Tang, H. Zhu, Y. Han, Q. Jiang, T. Li, X. Cao, and Z. Wang, *Nano Energy* **14**, 217 (2014).
- <sup>25</sup> G. Zhu, Y. Su, P. Bai, J. Chen, Q. Jing, W. Yang, and Z. L. Wang, *ACS Nano* **8**, 6031 (2014).
- <sup>26</sup> Z. H. Lin, G. Cheng, L. Lin, S. Lee, and Z. L. Wang, *Angew. Chemie-Int. Ed.* **52**, 12545 (2013).
- <sup>27</sup> P. Bai, G. Zhu, Z. H. Lin, Q. Jing, J. Chen, G. Zhang, J. Ma, and Z. L. Wang, *ACS Nano* **7**, 3713 (2013).
- <sup>28</sup> X. Pu, L. Li, H. Song, C. Du, Z. Zhao, C. Jiang, G. Cao, W. Hu, and Z. L. Wang, *Adv. Mater.* **27**, 2472 (2015).
- <sup>29</sup> Z. Tian, J. He, X. Chen, T. Wen, C. Zhai, Z. Zhang, J. Cho, X. Chou, and C. Xue, *RSC Adv.* **8**, 2950 (2018).
- <sup>30</sup> G. H. Lim, S. S. Kwak, N. Kwon, T. Kim, H. Kim, S. M. Kim, S. W. Kim, and B. Lim, *Nano Energy* **42**, 300 (2017).
- <sup>31</sup> Z. Tian, J. He, X. Chen, Z. Zhang, T. Wen, C. Zhai, J. Han, J. Mu, X. Hou, X. Chou, and C. Xue, *Nano Energy* **39**, 562 (2017).
- <sup>32</sup> Z. Zhang, J. He, T. Wen, C. Zhai, J. Han, J. Mu, W. Jia, B. Zhang, W. Zhang, X. Chou, and C. Xue, *Nano Energy* **33**, 88 (2017).
- <sup>33</sup> W. Song, B. Gan, T. Jiang, Y. Zhang, A. Yu, H. Yuan, N. Chen, C. Sun, and Z. L. Wang, *ACS Nano* **10**, 8097 (2016).
- <sup>34</sup> J. Chen, G. Zhu, W. Yang, Q. Jing, P. Bai, Y. Yang, T. C. Hou, and Z. L. Wang, *Adv. Mater.* **25**, 6094 (2013).
- <sup>35</sup> G. Cheng, Z. H. Lin, Z. Du, and Z. L. Wang, *Adv. Funct. Mater.* **24**, 2892 (2014).
- <sup>36</sup> S. Wang, L. Lin, and Z. L. Wang, *Nano Lett.* **12**, 6339 (2012).
- <sup>37</sup> X. S. Zhang, M. Di Han, R. X. Wang, B. Meng, F. Y. Zhu, X. M. Sun, W. Hu, W. Wang, Z. H. Li, and H. X. Zhang, *Nano Energy* **4**, 123 (2014).